FF

EUROPEAN ORGANIZATION FOR NUCLEAR RESEARCH
EUROPEAN LABORATORY FOR PARTICLE PHYSICS

CERN LIBRARIES, GENEVA
SCAN-9902067

CERN-TIS-99-003-RP-PP

Sw 9907

Radiation produced by the LEP superconducting RF cavities

M. Silari[(1)], S. Agosteo[(2)], J-C. Gaborit[(1)] and L. Ulrici[(1)]

[(1)] CERN, 1211 Geneva 23, Switzerland
[(2)] Politecnico di Milano, Dipartimento di Ingegneria Nucleare, Via Ponzio 34/3, 20133 Milan, Italy

Abstract

The LEP superconducting RF cavities present an important radiation source both during the conditioning and during normal working conditions. Before their installation in the accelerator the cavities are tested and conditioned in a laboratory bunker up to their maximum achievable field, which in some cases can be as high as 9 MV m^{-1}. This paper discusses radiation measurements carried out on both single cavities and standard 4-cavity modules. Following a brief description of the processes underlying the emission of radiation, the results of photon and neutron measurements are given. The induced radioactivity in various materials is also evaluated; shielding guidelines and radiation protection procedures are briefly discussed.

Submitted for publication in Nuclear Instruments and Methods A

CERN, Geneva, Switzerland
2 February 1999

1. Introduction

The CERN Large Electron Positron collider (LEP) [1] started operation in 1989; until 1995 it was operated at energies centred around 45.6 GeV per beam, to study the production of the Z^0 particle which has a mass of 91.2 GeV. During that phase the LEP acceleration system consisted of 128 copper radiofrequency (RF) cavities [1] installed in straight sections 2 and 6 (the collider has an eightfold symmetry with eight arcs and eight straight sections, for a total circumference of 26.658 km). The copper cavities were assembled in groups of 16 units, each powered by 2 klystrons. The klystrons are placed in auxiliary tunnels (conventionally called *klystron galleries*) running parallel to the machine tunnel; the klystron galleries are 210 m long and are shielded by 8 m of rock from the LEP tunnel, with a number of ducts for the waveguides traversing the shielding.

The end of 1995 marked the beginning of the LEP2 phase [2], with the progressive upgrade of the collider energy above the W pair production threshold [3], towards a goal of approximately 100 GeV per beam in 1999 and possibly a few GeV above in 2000, the last year of operation. The major modification to the accelerator is the addition of a completely new accelerating system employing superconducting RF cavities [4]. This new accelerating system, which adds to and partially replaces the normal conducting copper cavity system, consists of several modules, each one assembling four cavities. Each cavity has a total length of 1.7 m and is operated at 352.2 MHz (the same frequency of the copper RF system): it is made up of four half-wavelength long, quasi-spherical cells, made either of solid niobium or of OFHC (oxygen-free) copper coated with a thin niobium layer. Each cavity is surrounded by a cryostat containing 200 l of liquid helium for operation at 4.2 K and the whole assembly is contained in a vacuum vessel 255 cm long and 110 cm in diameter. Four of these vessels are coupled to make up a 4-cavity module with total length of 12.5 m. Each module is transported and installed in LEP as a whole.

The upgrade of LEP to LEP2 is being accomplished in steps, as detailed in Table 1. The superconducting modules are more or less equally distributed in the four straight sections; this has required the excavation of klystron galleries parallel to straight sections 4 and 8, similar to those already existing at points 2 and 6. By 1999 the accelerating system will consist of 48 normal conducting cavities, 272 Nb-film cavities and 16 Nb-sheet cavities (Table 2), for a total of 72 superconducting modules. The superconducting cavities and the related electronics are grouped in RF units consisting of 16 cavities, 2 klystrons and 22 electronics racks. Each unit works independently of the others. The RF system has the double purpose of ramping the beam from 22 GeV (the injection energy) to the energy value required for physics, and to compensate for the continuous energy loss due to synchrotron radiation during coasting. In fact most of the RF power is needed for this second task, as the energy lost by synchrotron radiation increases with the fourth power of the beam energy and at 100 GeV is therefore about 25 times larger than at 45 GeV.

The superconducting RF cavities are an important radiation source both during their conditioning before installation in LEP and during operation of the collider. In LEP the cavities are presently working just below their nominal electric field, to maintain a certain reserve of RF power which allows them to be driven to the nominal gradient in case two groups of eight cavities trip simultaneously [5]. Nonetheless before being installed in LEP the cavities are tested up to their maximum achievable field, which in some cases can be as high as 9 MV m^{-1}. This paper discusses radiation measurements carried out on both single cavities and 4-cavity modules. Following a brief description of the processes underlying the emission of radiation, the results of measurements of prompt photon and neutron radiation are given. In addition, some parts of the system become radioactive during operation; this phenomenon is described and the induced radioactivity in various materials is evaluated. Finally, shielding guidelines and radiation protection procedures are briefly discussed.

Table 1. Timetable of the installation of the superconducting RF modules in LEP.

Date	Energy (GeV)	Point 2	Point 4	Point 6	Point 8	Total
October 95	68	4	0	8	4	16
June 96	80.5	5	11	8	12	36
October 96	86	8	14	8	14	44
May 97	91.5	16	18	8	18	60
May 98	94.5	16	18	16	18	68
April 99	100.0 (*)	16	20	16	20	72

(*) Expected value

Table 2. Main parameters of LEP normal conducting and superconducting RF cavities. 16 superconducting cavities are made from solid niobium (Nb-sheet), the rest are made of copper coated with a niobium film.

Cavity type	Effective length (m)	Nominal accelerating gradient (MV m^{-1})	Nominal accelerating voltage (MV)
Cu	2.130	1.174	2.50
Nb-sheet	1.702	5.0	8.51
Nb-film	1.702	6.0	10.21

2. Radiation produced during RF conditioning and operation in LEP

At the beginning of LEP operation in 1989, the technology of superconducting accelerating systems was relatively young as the first machine employing it, the HEPL linac at University of Stanford, came into operation in 1977. The largest system in operation at the moment of LEP start-up was the 32 GeV e^+/e^- collider TRISTAN at KEK (Tsukuba, Japan); other accelerators are now running with superconducting RF cavities, such as HERA at DESY (Germany) and the Thomas Jefferson National Accelerator Facility in Newport News (Virginia, USA) [6]. The superconducting

technology for RF systems is now mature and will be used in future accelerators, such as the Large Hadron Collider (LHC) [7] and the TESLA e^+/e^- collider [8].

The LEP cavities were built by three European firms, Ansaldo (Italy), Cerca (France) and Siemens (Germany), and then brought to CERN for testing and acceptance. The tests consist in measuring their quality factor as a function of accelerating gradient. He-processing (i.e., conditioning the cavity in a He gas) or pulse power processing are carried out to improve cavity performance by cleaning its walls from impurities. If the processing does not produce satisfactory results the niobium layer is removed and the cavity is re-coated with a new niobium film. The performance is first measured on the bare cavity installed in a vertical test cryostat and then on the four-cavity module in a horizontal set-up. Final conditioning is carried out after the module has been installed in the LEP tunnel.

The production of radiation is mainly caused by field emission of electrons from small impurities on the Nb surface. Electron multipacting (a resonance phenomenon linked to the electric surface field, the secondary electron emission coefficient of the surface, the geometry of the cavity and the frequency) is a less important mechanism if the Nb surface is properly cleaned [9]. Heating of the cavity walls reduces the quality factor of the cavity (electron loading), a well known phenomenon observed in other superconducting cavity systems [10], and increase cryogenic losses. Trajectory calculations have shown that there are essentially two electrons sources [11,12]: 1) a high intensity source of low energy electrons mainly producing transverse bremsstrahlung X-rays; and 2) a low intensity source of high energy electrons travelling parallel to the cavity axis and generating X-rays emitted along the axis (Fig. 1). The latter source is more important, due to the much higher energy to which electrons can be accelerated to, up to the maximum field of the cavity. When these electrons strike the cavity walls or any other material (such as a stopper placed on the cavity axis during conditioning, or beam line elements downstream of the module during operation in LEP), they produce intense bremsstrahlung radiation. Part of this bremsstrahlung radiation is sufficiently energetic to induce photonuclear reactions resulting in neutron production and activation of material [13]. Some components close to the module extremities may become activated and in addition the thermal insulation may be damaged.

It should be underlined that each cavity has its own "history" and the conditioning process can vary significantly from one cavity to the other. However, mass spectrometry has shown that the spectrum of the electrons emitted and accelerated in a module has normally four peaks, more or less equally spaced, one corresponding to the maximum field, the others to ¼, ½ and ¾ of this maximum [14]. This spectral shape is in agreement with the second process mentioned above.

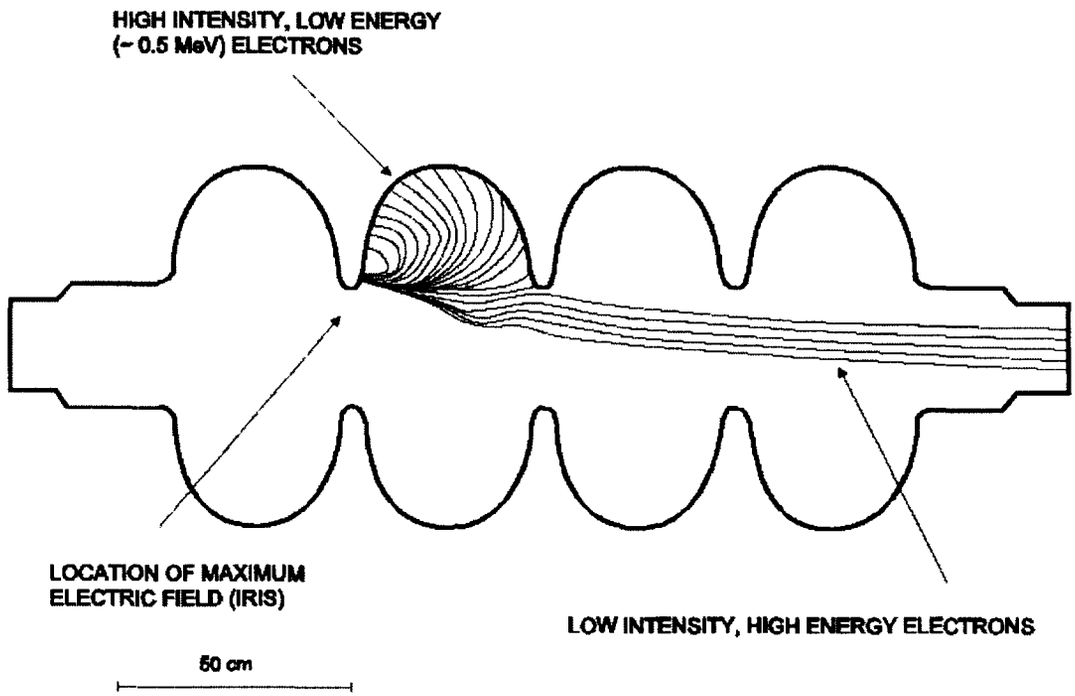

Fig. 1. Qualitative representation of trajectories of electrons produced by field emission and accelerated in the superconducting cavity

3. Radiation protection

Single cavities are tested in vertical bunkers which are 4.60 m in depth, with their upper part shielded by a sliding concrete plug 80 cm thick. The 4-cavity modules are tested in an horizontal set-up, shielded and equipped with interlocks for access. As one would expect and as it will be shown below, the photon radiation is dominant over the neutron component. The bunkers are built with concrete blocks of standard size. Side shielding is 160 cm and top shielding is 40-60 cm concrete. On the cavity axis shielding is provided by 80 cm barite concrete with the addition of 20-40 cm iron. In case of space constraints, 80 cm of iron proved to be sufficient. Access is via a 2-legs labyrinth, the first leg being 2 m long and the second one 3 m long. In addition, the access door is shielded with 2 cm of lead. The interlocks act directly on the klystrons or on the power supplies. A limited area around the bunkers is defined as Controlled Radiation Area (dose equivalent rate below 25 μSv h^{-1} under normal conditions and below 100 μSv h^{-1} under transient conditions), whilst the rest of the building is classified as Supervised Area (dose equivalent rate below 2.5 μSv h^{-1} and 7.5 μSv h^{-1}, respectively). With a module tested at 6.5 MV m^{-1} or 44 MV total field, the dose rate at the exit of the access maze can attain up to 15 μSv h^{-1}, which reduces to 3 μSv h^{-1} at 1 m distance.

A system of air-filled ionisation chambers connected to the general data logging system of the Radiation Protection group monitor the radiation levels and generate alarms if the dose rate exceeds a pre-defined threshold. The measured data are recorded in the data base of all CERN installed radiation monitors. The same type of

detectors are installed at both extremities of a module, at 40 cm distance from the cryostat, during its final conditioning in the LEP tunnel.

4. Radiation measurements

Measurements of the photon and neutron radiation were carried out during RF conditioning of single cavities and of four cavity modules, before their final installation in LEP. The measurements were generally carried out "parasitically", i.e. during the normal conditioning procedure, therefore with little control on the RF parameters. On the other hand, this has the advantage of giving an exact picture of the typical radiation environment during the process.

4. 1 Instrumentation

Photon measurements were performed with an ionisation chamber for high dose rates, namely a cylindrical PTW chamber with 31 mm diameter and 30 cm^3 volume, 1 mm wall and 3 mm build-up cap made of $(C_5H_8O_2)_n$, graphite-coated aluminium electrode, with measuring range from 30 keV to 50 MeV, interfaced to a PTW UNIDOS electrometer. Integrated doses were measured with polymer-alanine dosimeters. As the radiation field is dominated by the photon component (10^2 to 10^4 times more intense than neutrons in term of dose equivalent) and rem counters are not completely insensitive to gammas, neutron measurements were carried out only with passive-type detectors. Two techniques were used, i.e. commercial superheated drop (bubble) detectors [15] and activation foils.

Bubble detectors [16-18] are suspensions of over-expanded halocarbon and/or hydrocarbon droplets (about 100 μm in diameter) which vaporise upon exposure to the high LET recoils from neutron interactions. The superheated droplets are dispersed in a gel-like medium contained in a vial and act as continuously sensitive, miniature, bubble chambers. The total amount of vapour evolved from the radiation-induced nucleation of drops gives an integrated measure of the total neutron exposure. When calibrated with an Am-Be source, the dosimeter underestimates the ambient dose equivalent from thermal and intermediate neutrons, which was then determined with the activation technique discussed below. On the other hand, this device is completely insensitive to low LET radiation, X-rays and gammas, which is a clear advantage if one wants to measure the neutron component in a photon dominated field, as in the present case. The type of units employed are passive, integrating, pen-size dosimeters, temperature-compensated to give a uniform response within ± 20% in the interval 20°-37°, with an average sensitivity of 0.05 bubble per μSv over the energy range from 200 keV to 15 MeV. The bubbles are counted visually about half an hour after exposition.

The activation foil technique is useful to determine the neutron component in a mixed radiation field, from a measurement of the radionuclides that are produced by neutron-induced reactions in a thin foil of (usually) pure chemical composition. Once exposed, the foil is qualitatively and quantitatively analysed by gamma spectrometry. The neutron flux is obtained from the induced specific activity in the material from the

knowledge of the reaction cross-section. The limits of this technique are: 1) the photon component which is always associated to the neutron field can generate radionuclides interfering with those from neutron-induced reactions; 2) the threshold of most neutron induced-reactions is above a few MeV; 3) the cross-sections for threshold reactions for most materials are of the order of tens of mbarns and therefore measurable activation is only induced with quite large fast neutron fluence rates.

Gold and indium prove to be the best suited materials for neutron activation: the reactions exploited are $^{197}Au(n,\gamma)^{198}Au$ and $^{115}In(n,\gamma)^{116m}In$, respectively. The thermal and epithermal components of the neutron spectrum were discriminated by exposing the two types of foils both bare and under a cadmium cover. A 1/E behaviour was assumed for the epithermal component. The gamma spectrometry measurements of the irradiated foils were carried out by an Intertechnique HpGe detector (104 cm^3 sensitive volume, 22% relative efficiency at 1.33 MeV), powered by a Silena HV supply model 7716 and interfaced to a Silena spectroscopy amplifier model 7611/L.

In some cases ^{32}S activation detectors (disks 50 mm in diameter and 6 mm thick) were also used, exploiting the $^{32}S(n,p)^{32}P$ reaction which has a threshold at about 2 MeV; the cross section extends up to about 20 MeV and has its maximum (300 mb) in the interval 4 to 10 MeV [19]. However, due to the half-life (14.3 days) of the product this technique can only be employed if the measurement time is at least a few days and if the neutron field is sufficiently intense (i.e., if the module is particularly "bad" and generates a lot of radiation).

4. 2 Measurements on single RF cavity

Photon and neutron measurements were carried out on a number of cavities undergoing their first conditioning cycle (lasting about 24 hours) in the vertical test cryostat. The PTW ion chamber and bubble detectors were placed inside the top concrete shield, at about 10 cm distance from the cryostat cap; this cap is made of stainless steel 5 cm thick and therefore provides a partial shielding.

A typical behaviour of the photon dose rate as a function of time and of the electric field in the cavity is shown in Fig. 2. There is a sharp increase in the radiation emission when the electric field is raised from 6 MV m^{-1} to about 8.5 MV m^{-1}, followed by a slow decrease during the conditioning process. The conditioning reduces the radiation emitted by the cavity by about a factor of 5, and increases its quality factor. The strong dependence of radiation dose on the applied field is clearly seen in Fig. 3, presenting the photon dose rate as a function of electric field with and without He-processing. In this particular case there was virtually no difference in the emitted radiation with either mode, but each cavity has its own behaviour. Fig. 4 shows a similar plot for another unit, in which the influence of He-processing is clearly visible. From Figs. 3 and 4 one sees that there is a difference of a factor 5 to 6 in the maximum dose rate produced by the two units. In any case, the emission of radiation starts at a threshold between 5 and 6 MV m^{-1}, followed by a rapid increase.

A measurement of integrated neutron dose over the 24 hour conditioning time gave an average dose rate of 7.1 ± 2 μSv h^{-1}. This value is about 10^{-4} smaller than the photon dose rate.

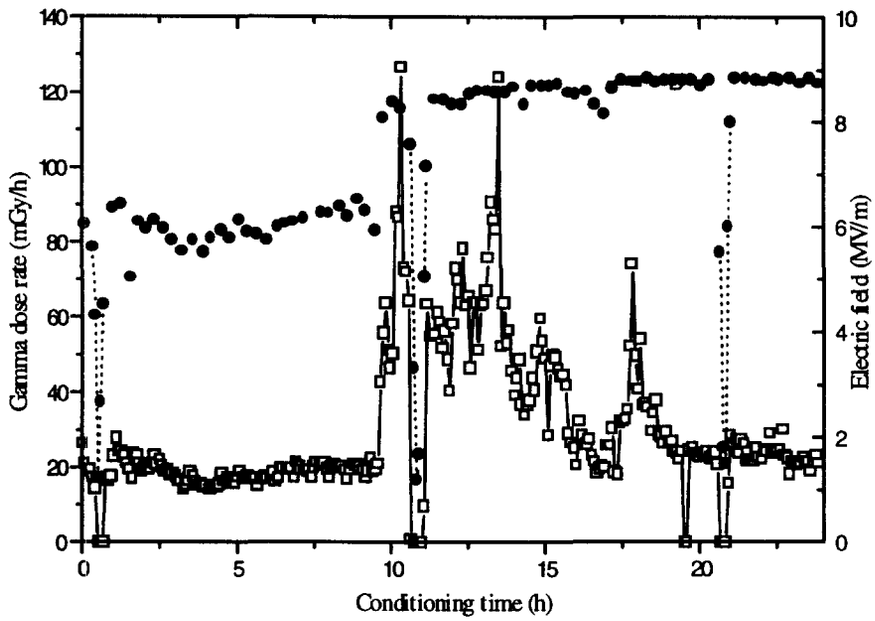

Fig. 2. Photon dose rate (open squares, left vertical axis) from a superconducting cavity during the first 24 hours of conditioning, as a function of the applied field (full circles, right vertical axis).

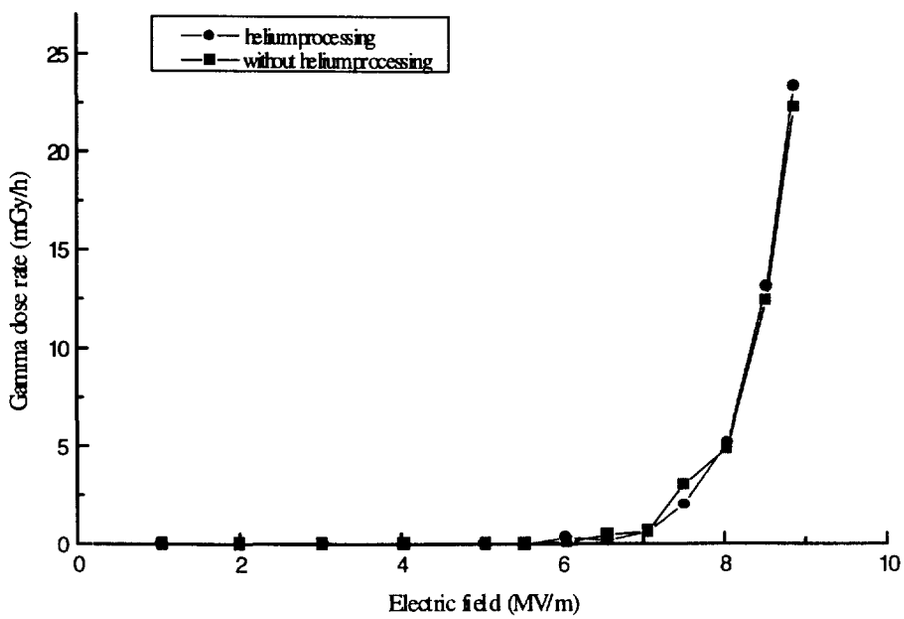

Fig. 3. Photon dose rate as a function of applied electric field, with and without helium processing.

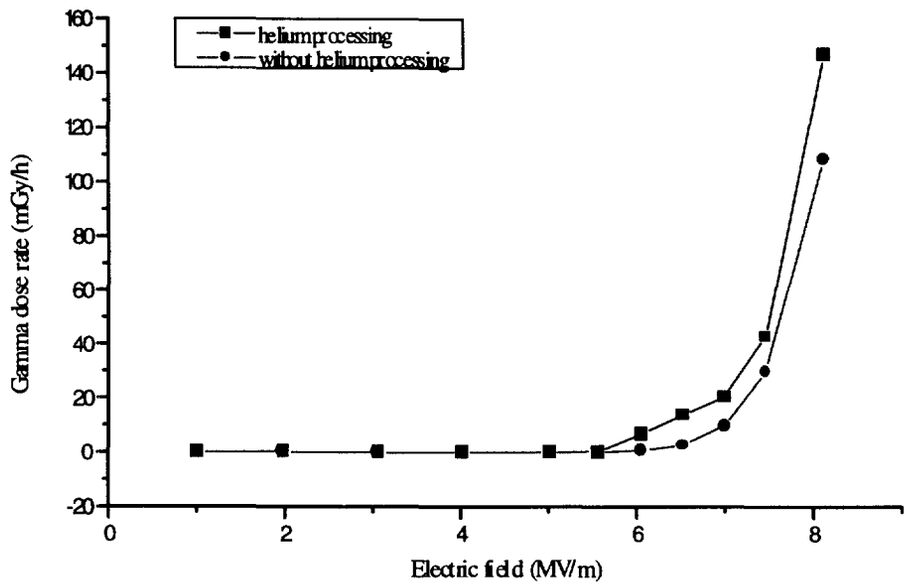

Fig. 4. Photon dose rate as a function of applied electric field, with and without helium processing, for a different unit.

4.3 Measurements on 4-cavity modules

Once 4 cavities are assembled in a module, the unit is again tested in a laboratory bunker. If this test is satisfactory, the module is installed in the LEP tunnel where it undergoes final conditioning. The conditioning process in the laboratory varies from unit to unit and may be protracted for several days or weeks. The first conditioning cycle of a module usually lasts 24 hours; the total electric field is normally set at about 40 MV (klystron power equal to about 150 MW), but this may vary substantially according to the status of the equipment. Although each cavity in the module has already been conditioned at least once, the dose rates measured at the extremities of a module (by both the PTW ion chamber and alanine dosimeters) are much higher than for a single cavity, as the total field is a factor of 4 higher (and there is no local shielding, as the measurements are done inside the bunker). The dose rates at the two ends of the module are usually different, in some cases by as much as two orders of magnitude. Measurements carried out on several modules with an applied electric field in the range 30-45 MV have shown that the photon dose rate on the axis, close to the exit cone, varies considerably from unit to unit, ranging from a few Gy h^{-1} up to a few thousands Gy h^{-1}. In general, the first modules were much worse with respect to their radiation emission than those built more recently.

Neutron measurements were carried out on one module, to assess the contribution of neutrons (thermal, epithermal and fast) to the total dose equivalent. Bubble detectors were placed at 50 cm distance from the extremity of the module, at 0°, 45° and 90° with respect to its axis. Simultaneous measurements with the PTW ionisation chamber in the same positions showed that the ratios between the fast (above 100 keV) neutron dose equivalent and the photon dose was 3.5×10^{-3} at 0°, 1.7×10^{-3} at 45° and 1.5×10^{-3} at 90°.

The thermal and epithermal neutron fluence rates were evaluated with activation foils placed at 50 cm distance from the cryostat, at 45° with respect to its axis. Gold and indium gave the same results within the experimental uncertainties: 51.2 ± 2.2 cm^{-2} s^{-1} and 55.1 ± 4.7 cm^{-2} s^{-1} for the thermal component and 23.6 ± 0.9 cm^{-2} s^{-1} and 25.6 ± 2.0 cm^{-2} s^{-1} for the epithermal component, respectively. Using an average fluence to dose equivalent conversion factor $H^*(10)/\Phi$ of 10 pSv cm^2 and 20 pSv cm^2 for the thermal and epithermal components, respectively [20], and normalising the above values to the photon dose rate measured in the same position by the PTW chamber (390 mSv h^{-1}), one obtains that the ratio of the thermal and epithermal dose equivalent values to the photon dose are both about $5x10^{-6}$, hence negligible with respect to the fast neutron contribution.

In another case, on a module operated at about 50 MV and generating much more radiation, neutron measurements performed on the axis with ^{32}S activation detectors gave fluence rates of $1.5x10^3$ cm^{-2} s^{-1} and $8x10^3$ cm^{-2} s^{-1} at about 1 m distance from the two ends. These values correspond to a fast (above 2 MeV) neutron dose rate of about 2 mSv h^{-1} and 10 mSv h^{-1}, respectively. This results in a ratio of neutron to photon doses, the latter determined by alanine dosimetry, of approximately 10^{-3}, in agreement with the figure above.

It is interesting to compare the present measurements of the neutron component with measurements of neutron "contamination" carried out around medical electron accelerators employed in cancer radiation therapy, operating at about the same field (typically 10-25 MV). Bourgois et al. [21] have measured neutron dose equivalent values of between 0.25 and 7.5 mSv Gy^{-1} (neutron dose equivalent per 1 Gy of therapeutic photon dose) at the beam isocentre for photons of 8 to 25 MV. Kase et al. [22] have determined by both Monte Carlo calculations and measurements the neutron fluence at various locations around a medical linac operated at 10, 15, 18 and 20 MV. Converting the fluence to dose equivalent one obtains about $6x10^{-2}$ mSv Gy^{-1} to 0.2 mSv Gy^{-1}(at the isocentre) for operation at 10 MV and 4 mSv Gy^{-1} to 6 mSv Gy^{-1} (at the isocentre) for operation at 20 MV. LaRiviere [23] has measured values of between 1.4 and 5.8 mSv Gy^{-1} at 1 to 5 m distance, respectively, from the isocentre of a 24 MV linac. Tosi et al. [24] have performed neutron measurements around 15 MV and 25 MV linacs and a 21 MV microtron. They have reported values of 15 to 0.1 mSv Gy^{-1} for the 15 MV linac and of 7.2 to 0.45 mSv Gy^{-1} for the 25 MV linac, for distances of 5 to 250 cm from the isocentre, respectively. These literature results are in good agreement with those discussed here.

5. Induced radioactivity

During conditioning in a laboratory bunker, the vacuum valves situated at the two extremities of a module are kept open, in order to avoid that they are radiation damaged. The two ends of the vacuum chamber are closed by stainless steel vacuum flanges. The electrons are absorbed by a copper block placed in the vacuum on the cavity axis, installed in between the valve and the flange. Both the copper block and

the flange undergo activation, where the level strongly depends on the unit under test. The residual dose rate at 10 cm distance from these components may reach several mSv h^{-1} a few minutes after the module has been switched off. It was found that the dose rate decreases by about a factor of 10 in 40 minutes, due to the decay of short-lived radionuclides, followed by a much slower decrease (another factor of 10 in about 48 hours).

Gamma spectrometry measurements of the copper block and the stainless steel (type 316L) flange carried out several days after irradiation have identified several radionuclides: ^{51}Cr, ^{54}Mn, ^{56}Co, ^{57}Co, ^{58}Co, ^{60}Co, ^{65}Zn, ^{72}Se, ^{75}Se, ^{74}As, ^{120}Sb in copper; ^{48}V, ^{51}Cr, ^{52}Mn, ^{54}Mn, ^{56}Ni, ^{57}Ni, ^{56}Co, ^{57}Co, ^{58}Co, ^{60}Co, ^{88}Y, ^{92m}Nb, ^{95}Nb, ^{99}Mo in stainless steel. More details are given in the Appendix: the composition of stainless steel and copper are given in Tables A.1 and A.2; half-lives, main emissions and the production reactions of the various radionuclides detected are listed in Tables A.3 and A.4. The gamma-ray spectra of the two samples are shown in Figs. A.1 and A.2. The production reactions of the short-lived radionuclides responsible for most of the induced radioactivity in stainless steel 316L and OFHC copper in the first few minutes after the RF has been switched off can be supposed from the material composition given in Tables A.1 and A.2. In stainless steel, the activity would mainly come from $^{50}Cr(\gamma,n)^{49}Cr$ (half-life 42.1 min), $^{54}Fe(\gamma,n)^{53}Fe$ (8.51 min), $^{54}Fe(\gamma,n)^{53m}Fe$ (2.6 min), $^{92}Mo(\gamma,n)^{91m}Mo$ (1.09 min) and $^{92}Mo(\gamma,n)^{91}Mo$ (15.49 min); in copper, from the two reactions $^{63}Cu(\gamma,n)^{62}Cu$ (half-life 9.74 min) and $^{63}Cu(\gamma,3n)^{60}Cu$ (23.2 min).

In one case (module no. 2004) the thermic insulation was severely damaged by radiation and fell into pieces when the module was opened for maintenance. The insulation is constituted of several films of polyethylene terephthalate (PET) on which a thin aluminium layer (400 A) is deposited separated by a thick insulating layer made of polyester. A gamma-spectrometry analysis carried out on a sample taken from the damaged insulation has shown traces of ^{22}Na, ^{46}Sc, ^{51}Cr, ^{54}Mn and ^{65}Zn, most likely produced on impurities in the aluminium.

Experience has shown that during operation in LEP, only a few, well localised "spots" of induced radioactivity are produced on one or both extremities of the modules and/or on the vacuum valves immediately downstream. No induced radioactivity had ever been detected alongside a module. These "hot spots" are obviously generated by the stray electrons produced by the second mechanism discussed in section 2.

6. Conclusions

The RF system has proved extremely reliable during its routine operation in LEP over several years. It has been shown that the superconducting RF cavities can be driven for prolonged periods to a gradient considerably higher than their nominal average value of 6 MV m^{-1} used until now in LEP operation. In fact, a number of cavities already operate at a higher field, in order to compensate for the less

performing equipment. During the next (and last) two years of LEP lifetime, the collider energy will be raised to 100 GeV in 1999 and possibly a few GeV above in year 2000. This last step has to be achieved by exploiting the "reserve" in RF power still available, i.e. increasing the average accelerating gradient by about 1 MV m^{-1}. This will be made possible by an upgrade of the LEP cryogenic plants in order to provide more cooling power to the cavities, and by further development work to reduce the field emission and avoid excessive radiation levels. From the data presented in the present paper one expects an increase by a factor of two in the radiation emission. The situation will be closely watched.

Acknowledgements

We are indebted to G. Geschonke, O. Brunner and A. Cujious of the RF group for allowing us to perform the measurements and for many useful discussions. We also wish to thank F. Pirotte, D. Boulicault and R. Sanfilippo for their help with some of the measurements.

References

[1] LEP Design Report, Vol. II, The LEP main ring, CERN-LEP/84-01 (1984).

[2] LEP Design Report, Vol. III, LEP 2, CERN AC/96-01 (LEP2) (1996).

[3] L. Rolandi, Aim for LEP2 performance, Proceedings of the Fourth Workshop on LEP Performance, Chamonix (France), 17-21 January 1994, J. Poole ed., CERN SL/94-06 (DI) (1994), pp. 379-382.

[4] LEP Design Report, Vol. III, LEP 2, CERN AC/96-01 (LEP2) (1996), pp. 61-96.

[5] O. Brunner, RF system reliability and performance in 1997, Proceedings of the Eighth Workshop on LEP Performance, Chamonix (France), 27-30 January 1998, J. Poole ed., CERN SL/98-006 DI (1998), pp. 154-157.

[6] J. Tückmantel, World-wide superconducting cavity performance survey, Proceedings of the First Workshop on LEP Performance, Chamonix (France), 13-19 January 1991, J. Poole ed., CERN SL/91-23 (DI) (1991), pp. 393-402.

[7] The Large Hadron Collider, Conceptual Design, CERN/AC/95-05 (LHC) (1995).

[8] J. Ellis, E. Keil and G. Rolandi, Options for future colliders at CERN, CERN-EP/98-03 (1998).

[9] W. Weingarten, Superconducting cavities, in: CAS RF Engineering for particle accelerators, CERN 92-03 (1992), pp. 318-348.

[10] D. Dotson, M. Drury, R. May and C. Reece. Use of simple routine X-ray measurements in the performance analysis of cryogenic RF accelerator cavities, Health Physics of Radiation-Generating Machines, Proceedings of the 30th Midyear Topical Meeting, 5-8 January 1997, S. Josè, California, USA, Health Physics Society (1997), pp 213-218.

[11] H. Lengeler, X-ray radiation from a module of 4 superconducting cavities, Technical Note CERN/EF/4420H/H/ed (1989).

[12] H. Lengeler, Radiation protection of measuring set-ups for LEP 4-cell cavity, Technical Note CERN/EF/4370H/HL/ed (1989).

[13] W.P. Swanson, Radiological Safety Aspects of the Operation of Electron Linear Accelerators, Technical Report Series No.188, IAEA, Vienna (1979).

[14] O. Brunner, private communication.

[15] Neutron bubble detectors type BD PND, Bubble Technology Industries, Inc., Chalk River, Ontario, Canada.

[16] R.E. Apfel, The superheated drop detector. Nucl. Instr. and Meth. 162 (1979) 603-608.

[17] F. d'Errico and W.G. Alberts, Superheated-drop (bubble) neutron detectors and their compliance with ICRP-60. Radiat. Prot. Dosim. 54 (1994) 357-360.

[18] F. d'Errico, W.G. Alberts and M. Matzke, Advances in superheated drop (bubble) detector techniques. Radiat. Prot. Dosim. 70 (1997) 103-108.

[19] V. McLane, C.L. Dunford and P.F. Rose, Neutron cross sections, Vol. 2, Academic Press (1988).

[20] International Commission on Radiological Protection, ICRP Publication 74, Conversion coefficients for use in radiological protection against external radiation, Pergamon Press (1996).

[21] L. Bourgois, D. Delacroix and A. Ostrowsky, Use of bubble detectors to measure neutron contamination of a medical accelerator photon beam, Radiat. Prot. Dosim. 74 (1997) 239-246.

[22] K.R. Kase, X.S. Mao, W.R. Nelson, J.C. Liu, J.H. Kleck and M. Elsalim, Neutron fluence and energy spectra around the Varian Clinac 2100/2300C medical accelerator, Health Phys. 74 (1998) 38-47.

[23] P.D. LaRiviere, Neutron energies in medical electron accelerator rooms, Med. Phys. 12 (1985) 769-775.

[24] G. Tosi, A. Torresin, S. Agosteo, A. Foglio Para, V. Sangiust, L. Zeni and M. Silari, Neutron measurements around medical electron accelerators by active and passive detection techniques, Med. Phys. 18 (1991) 54-60.

[25] E. Brown and R.B. Firestone, Table of radioactive isotopes, V.S. Shirley, editor, John Wiley & Sons (1986).

APPENDIX

The composition of stainless steel 316L of the vacuum valves and that of copper constituting the stoppers is given in Tables A.1 and A.2. The radionuclides identified by gamma-spectrometry in the two materials are listed in Tables A.3 and A.4 with their half-lives, their principal gamma emissions and the most probable production reactions. The gamma-ray spectra of the two samples are shown in Figs. A.1 and A.2.

Table A.1. Composition of stainless steel 316L. The rest is iron.

Element	Cr	Ni	C	Si	Mn	Mo	N	P	S	Co
Composition (%)	16-18.5	11-14	0.03 max	1 max	2 max	2-2.5 max	0.05 max	0.03 max	0.01 max	0.22 max

Table A.2. Maximum content of trace impurities in copper OFHC. The percent content of copper is 99.99%. The total of the seven elements As, Sb, Bi, Se, Te, Sn and Mn does not exceed 40 ppm.

Element	Ca	P	S	Zn	Hg	Pb	Se	Te	Bi	O
Composition (ppm)	1	3	18	1	1	10	10	10	10	10

Table A.3. Main emissions detected in the gamma spectrometry [25] and possible production reactions (listed in order of decreasing importance) of the radionuclides found in stainless steel 316L taken from module No. 2017.

Radionuclide	Half-life	Main emissions in keV (%)	Production reactions
^{48}V	15.98 d	983.5 (100) 1312.0 (97.5) 2240.3 (2.41)	$^{50}Cr(\gamma,pn)$
^{51}Cr	27.7 d	320.1 (9.83)	$^{52}Cr(\gamma,n)$ $^{53}Cr(\gamma,2n)$ $^{54}Cr(\gamma,3n)$
^{52}Mn	5.59 d	744.2 (90) 935.5 (94.5) 1434.1 (100)	$^{55}Mn(\gamma,3n)$ $^{54}Fe(\gamma,pn)$
^{54}Mn	312.2 d	834.8 (100)	$^{55}Mn(\gamma,n)$ $^{56}Fe(\gamma,pn)$
^{56}Ni	6.1 d	750.0 (49.5) 811.9 (86) 1561.8 (14)	$^{58}Ni(\gamma,2n)$
^{57}Ni	1.5 d	1377.6 (77.9) 1919.4 (14.7)	$^{58}Ni(\gamma,n)$ $^{60}Ni(\gamma,3n)$
^{56}Co	78.76 d	846.8 (99.9) 977.6 (1.4) 1037.8 (14.1) 1238.3 (67) 1771.4 (15.5) 2015.4 (3.03) 2034.9 (7.78) 2598.6 (16.8) 3009.7 (1.03)	$^{58}Ni(\gamma,pn)$ $^{59}Co(\gamma,3n)$
^{57}Co	271.3 d	122.1 (85.5) 136.5 (10.7)	$^{58}Ni(\gamma,p)$ $^{59}Co(\gamma,2n)$ $^{60}Ni(\gamma,p2n)$
^{58}Co	70.91 d	810.8 (99.4)	$^{59}Co(\gamma,n)$ $^{60}Ni(\gamma,pn)$
^{60}Co	5.272 y	1173.2 (99.9) 1332.5 (100)	$^{61}Ni(\gamma,p)$ $^{62}Ni(\gamma,pn)$ $^{59}Co(n,\gamma)$
^{88}Y	106.6 d	898.1 (92.7) 1836.1 (99.4)	$^{89}Y(\gamma,n)$ (1)
$^{91}Nb^{m}$	62 d	1204.8 (3.5)	$^{92}Mo(\gamma,p)$ $^{94}Mo(\gamma,p2n)$
$^{92}Nb^{m}$	10.15 d	934.5 (99.0)	$^{94}Mo(\gamma,pn)$ $^{95}Mo(\gamma,p2n)$
^{95}Nb	34.97 d	765.8 (99.8)	$^{96}Mo(\gamma,p)$ $^{97}Mo(\gamma,pn)$ $^{98}Mo(\gamma,p2n)$
^{99}Mo	2.75 d	140.5 (90.7)	$^{100}Mo(\gamma,n)$

(1) The presence of ^{88}Y can only be explained by traces (<0.01%) of natural Yttrium in the material.

Table A.4. Main emissions detected in the gamma spectrometry [25] and possible production reactions (listed in order of decreasing importance) of the radionuclides found in OFHC copper.

Radionuclide	Half-life	Main emissions in keV (%)	Production reactions
^{51}Cr	27.7 d	320.1 (9.83)	$^{52}Cr(\gamma,n)$ (1)
^{54}Mn	312.5 d	834.8 (100)	$^{55}Mn(\gamma,n)$
^{56}Co	78.76 d	846.8 (99.9) 1037.8 (14.1) 1238.3 (67) 1771.4 (15.5) 2034.9 (7.78) 2598.6 (16.8)	$^{58}Ni(\gamma,pn)$ $^{59}Co(\gamma,3n)$ (2)
^{57}Co	271.5 d	122.1 (85.5) 136.5 (10.7)	$^{58}Ni(\gamma,p)$ $^{59}Co(\gamma,2n)$ (2) $^{60}Ni(\gamma,p2n)$
^{58}Co	70.78 d	810.8 (99.4)	$^{59}Co(\gamma,n)$ $^{60}Ni(\gamma,pn)$ (2)
^{60}Co	5.272 y	1173.2 (99.9) 1332.5 (100)	$^{61}Ni(\gamma,p)$ $^{62}Ni(\gamma,pn)$ (2) $^{59}Co(n,\gamma)$ $^{63}Cu(\gamma,2pn)$
^{65}Zn	244.1 d	1115.5 (50.7)	$^{66}Zn(\gamma,n)$ $^{67}Zn(\gamma,2n)$ $^{68}Zn(\gamma,3n)$
^{72}Se	8.4 d	834.0 (91.3)	$^{74}Se(\gamma,2n)$
^{75}Se	119.77 d	121.1 (17.3) 136.0 (59)	$^{76}Se(\gamma,n)$ $^{77}Se(\gamma,2n)$ $^{78}Se(\gamma,3n)$
^{74}As	17.78 d	595.9(60.2) 634.8 (15.4)	$^{75}As(\gamma,n)$ $^{76}Se(\gamma,pn)$ $^{77}Se(\gamma,p2n)$
^{120}Sb	5.76 d	1113.4 (1.30) 1171.4 (100)	$^{121}Sb(\gamma,n)$ $^{123}Sb(\gamma,3n)$ $^{122}Te(\gamma,pn)$

(1) The presence of ^{51}Cr can only be explained by traces of natural cromium in the material.

(2) The presence of cobalt radionuclides can generally only be explained by traces of natural cobalt or nichel in the material.

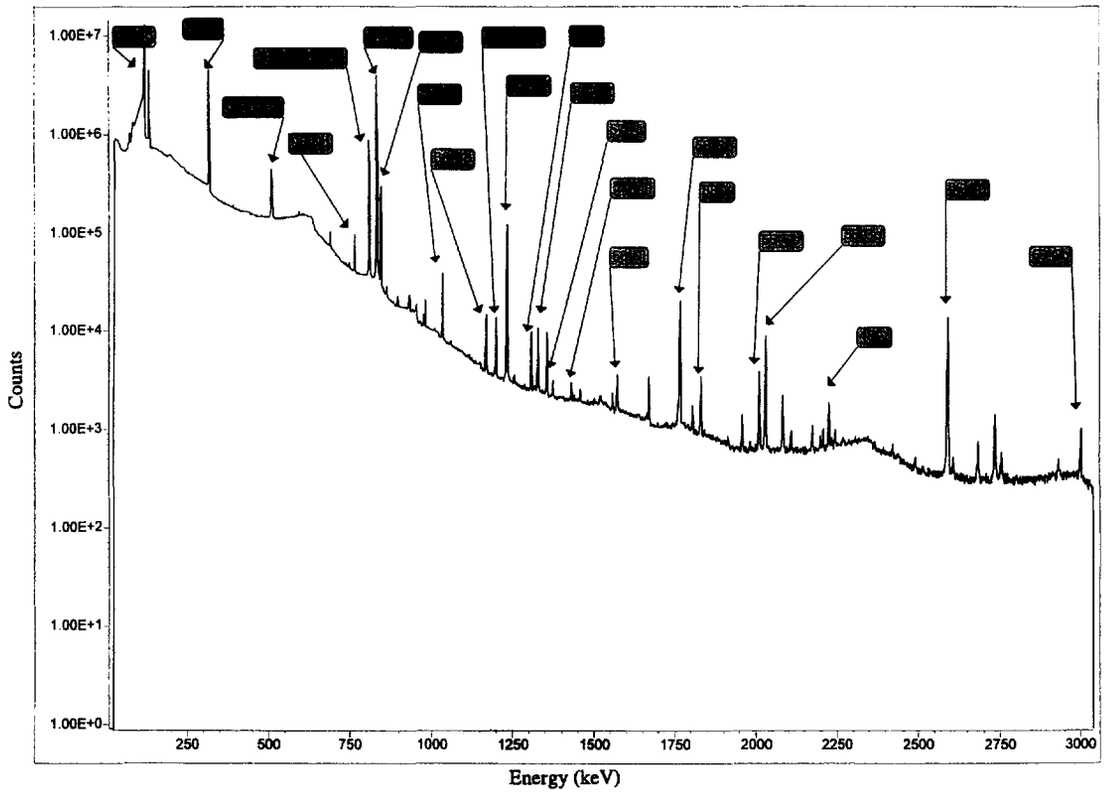

Fig. A.1. Gamma-ray spectrum of stainless steel 316L irradiated during RF conditioning.

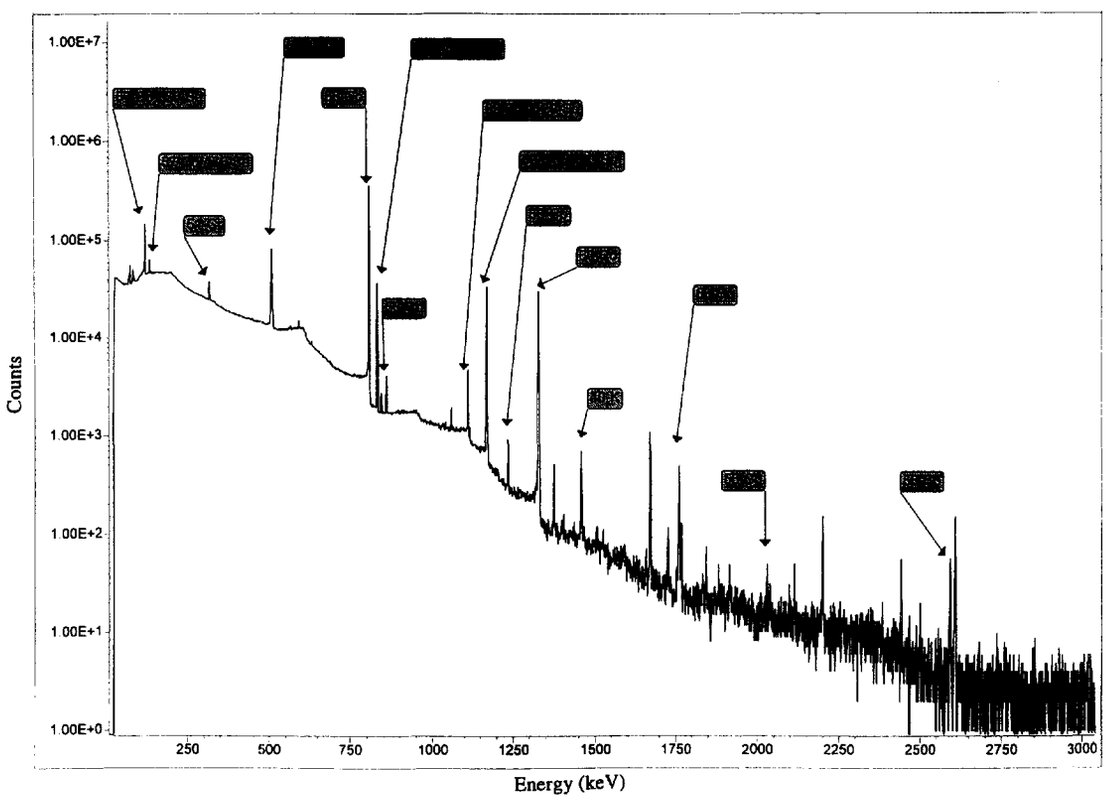

Fig. A.2. Gamma-ray spectrum of OFHC copper irradiated during RF conditioning.